Cross-slot extensional rheometry and the steady-state extensional response of long chain branched polymer melts

D. AuhlD. M. HoyleD. HassellT. D. LordO. G. HarlenM. R. MackleyT. C. B. McLeish

Citation: Journal of Rheology **55**, 875 (2011); doi: 10.1122/1.3589972
View online: http://dx.doi.org/10.1122/1.3589972
View Table of Contents: http://sor.scitation.org/toc/jor/55/4
Published by the The Society of Rheology

Cross-slot extensional rheometry and the steady-state extensional response of long chain branched polymer melts

D. Auhl

Institute of Condensed Matter, Bio- and Soft Matter, Université Catholique de Louvain, Louvain-la-Neuve B-1348, Belgium and Interdisciplinary Research Centre for Polymer Science and Technology (IRC), University of Leeds, Leeds LS2 9JT, United Kingdom

D. M. Hoyle

Department of Chemistry, University of Durham, Durham DH1 3LE, United Kingdom and Department of Applied Mathematics, University of Leeds, Leeds LS2 9JT, United Kingdom

D. Hassell

Department of Chemical Engineering, University of Cambridge, Cambridge CB2 3RA, United Kingdom and Department of Chemical and Environmental Engineering, University of Nottingham, Malaysian Campus, 43500 Semenyih, Malaysia

T. D. Lord

Department of Chemical Engineering, University of Cambridge, Cambridge, CB2 3RA, United Kingdom

O. G. Harlen[a)]

Department of Applied Mathematics, University of Leeds, Leeds LS2 9JT, United Kingdom

M. R. Mackley

Department of Chemical Engineering, University of Cambridge, Cambridge, CB2 3RA, United Kingdom

T. C. B. McLeish

Department of Physics, Durham University, Durham, DH1 3HP, United Kingdom

(Received 18 September 2010; final revision received 12 April 2011; published 20 May 2011)

[a)]Electronic mail: o.g.harlen@leeds.ac.uk

Synopsis

Stress-optical measurements at a flow stagnation point in confined geometries such as the cross-slot provide an elegant way to perform extensional testing for polymer melts. This technique is especially useful for samples which have a steady-state that cannot be reached (easily) in standard elongational rheometry, for example, highly branched polymers which show a non-homogeneous deformation that occurs in stretching experiments for Hencky strains above 4. In contrast to filament stretching, the cross-slot provides one point at which steady-state extensional flow may be sustained indefinitely. In this study, a Cambridge multi-pass rheometer [Coventry, K. D., and M. R. Mackley, J. Rheol. **52**, 401–415 (2008)] is used to generate planar elongational flow in a cross-slot geometry for different polyethylene melts. The experimental results are compared to finite element flow simulations using the multi-mode Pompom constitutive equations. The steady-state elongational viscosity at the stagnation point is computed from the flow-induced stress birefringence and the strain-rate determined from numerical calculations of the flow field. We apply this technique to a range of different branched high- and low-density polyethylene melts. This demonstrates both the effectiveness of this technique and shows how the stress distribution in a complex flow depends on molecular structure. Cross slot extensional rheometry therefore provides a very promising technique for parameterizing molecular constitutive equations for LCB melts.Extensional rheometry, Polymer melts, Polyethylene, Birefringence, Flow modeling, © *2011 The Society of Rheology.* [DOI: 10.1122/1.3589972]

I. INTRODUCTION

An accurate description of the elongational stress-strain relationship is required both for understanding polymer chain dynamics and for optimizing the processing performance of thermoplastic polymers. Elongational "viscosity" (more properly "stress growth coefficient") is a material function determined from a homogeneous extensional flow and is often used in addition to shear flow properties in characterizing materials. This flow type is stronger than shear flows as it orients chains in the direction of extension, allowing the development of large viscoelastic stresses in the fluid, and so provides a challenging test for molecular theories [Bent *et al.* (2003)]. Usually, the discussion of the elongational flow behavior is focused on "strain hardening," which describes the rise of the tensile stress growth coefficient above the linear viscoelastic reference case that is predicted by the Boltzmann superposition principle [Dealy (1990)]. From a practical point of view, this upturn is of great importance in many processing operations involving extension, for example, fiber spinning, film extrusion, and blow molding, since it has been proven to have a positive effect on the homogeneity of the processing deformation [Ide and White (1978); Münstedt *et al.* (1998)]. Furthermore, it can be used as a very sensitive tool for the molecular characterization of polymers regarding their chain architecture [Gabriel and Münstedt (2003); Münstedt and Laun (1981)]. Consequently, the measurement of elongational stresses in well controlled flows have been a subject of considerable effort, particularly in start-up. However, in spite of great advances in extensional rheometry over the past 2 decades, it many remains unclear whether or not the reported results reflect the true material behavior at a steady-state elongational flow [McKinley and Sridhar (2002)]. More recently Bach *et al.* (2003); Rasmussen *et al.* (2005) developed a filament stretching rheometer capable of reaching Hencky strains of around 7. For some low density polyethylene (LDPE) samples, the authors were able to achieve steady-state measurements, but only for a limited number of strain-rates.

Various techniques have been developed for measuring elongational flow properties of polymeric fluids. Simple elongational flow is commonly achieved by uniaxial stretching [e.g., Cogswell (1972); Meissner (1971); Meissner and Hostettler (1994); Sridhar *et al.* (1991); Münstedt (1979)]. In a series of papers Meissner, Münstedt, and Laun and co-workers investigated the strain-rate and stress dependence of the elongational viscosity as well as the recoverable strain in the steady-state for LDPE melts [for example, Laun and Münstedt (1976, 1978); Raible *et al.* (1979)]. These constant strain-rate tests were performed on low-density polyethylene samples using a Meissner-type elongational rheometer with rotating clamps. These tests indicated that the tensile stress runs through a broad maximum as a function of strain but does not saturate until Hencky strains ε_H of about 7. This effect was found to be even more pronounced at higher the strain-rates. However, Münstedt and Laun (1981) who used the same Meissner-type apparatus, suggested that the stress maximum may be an artifact because in the case of decreasing stress at high elongation the sample homogeneity became insufficient. Also, in subsequent studies, steady-state elongational viscosities were determined by creep tests in elongation [e.g., by Münstedt and Auhl (2005) for linear and long-chain branched polypropylenes using a Münstedt type tensile rheometer]. In comparison to stretching experiments, a steady-state flow in elongation can already be reached in creep experiments for smaller Hencky strains. The steady-state values are independent of the flow type by which they are obtained and can be used to evaluate whether the maximum values from constant strain-rate experiments are the steady-state values. From the prescribed constant stress and the resulting steady-state elongational rate, the steady-state elongational viscosities were compared to the maximum viscosities from stressing experiments. The results were similar in case of the linear and weakly branched materials but somewhat higher for the material with highest long-chain branching. Recently, Hassager and co-workers [Bach *et al.* (2003); Rasmussen *et al.* (2005)] reported an elongational viscosity overshoot for low-density polyethylenes using a filament rheometer with active feedback. However, even with active feedback a steady-state flow condition is difficult to establish in filament stretching flows (see for instance McKinley and Sridhar (2002)) since a large deformation is required and the sample cross-sections become very small and thus prone to inhomogeneities.

Stretching devices have also been developed to measure the response of materials to planar extensional flow Laun and Schuch (1989); Meissner (1981, 1982). In the linear viscoelastic limit, the extensional viscosities for these two flow types differ by a factor of 4/3. However, this difference decreases in the nonlinear strain hardened regime where the stress response tends to the same steady-state values, as seen, for example, in the LDPE measurements of Laun and Schuch (1989), which is captured by the multimode Pompom model of Inkson *et al.* (1999). Consequently, in this paper, we shall compare uniaxial and planar extensional data.

Apparatus designed to generate elongational flow around a stagnation point was initially pioneered by Taylor in a four roll mill [Taylor (1934)]. The technique has subsequently been used by numerous authors to interrogate polymer behavior in extensional flow, e.g., Coventry and Mackley (2008); Crowley *et al.* (1976); Frank and Mackley (1976); Janeschitz-Kriegl (1983); Macosko *et al.* (1980); Schoonen *et al.* (1998); Scrivener *et al.* (1979); Soulages *et al.* (2008); Verbeeten *et al.* (2001); Winter and Macosko (2009). Provided that the stagnation point remains fixed, material at this point experiences steady pure planar elongational flow. Compared to filament stretching flows, the stagnation point geometries have the advantage that elongational properties can be investigated without a disturbance from a potentially unstable free surface flow [Minoshima and White (1986)]. However, the flow history at other points in flow is more complex and

so only at the stagnation point is the stress the result of simple planar elongational flow. Müller *et al.* (1988) developed a technique based on opposed jets that is capable of measuring the effective extensional viscosity through monitoring the flow birefringence. Flow-induced birefringence as a rheo-optical technique allows the extraction of information about the stress distribution as well as the chain-stretch and chain-orientation conditions for polymeric fluids. From the change in the local refractive index of optically anisotropic monomer units, the orientation and stretch of polymer chains can be inferred. These rheo-optical measurements constitute a non-invasive rheological method, which can be applied to different and even very complex geometries during flow [Coventry and Mackley (2008); Hassell *et al.* (2009, 2008)].

In order to function quantitatively, it is necessary that the stress-optical rule familiar in linear response extends to non-linear deformations in some regime at least. Fortunately, simultaneous measurements of the tensile stress and birefringence as a function of time at constant tensile strain rate [for LDPE performed by Kotaka *et al.* (1997) and for polystyrenes by Venerus and Zhu (1999)] indicated that a linear stress-optical rule can be assumed up to about 1 MPa in the case of polyethylene. Koyama and Ishizuka (1989) performed rheo-optical measurements in elongation on molten commercial LDPE using a Meissner-type elongational rheometer (RME). They found a linear stress-birefringence relationship in the birefringent patterns, even when strain- hardening is seen in the non-linear elongational viscosity. Recently, Schuberth and Münstedt (2008) described an optical rheometer to simultaneously measure the velocity as well as stress distributions in a slit die using laser-Doppler velocimetry (LDV) and flow-induced birefringence (FIB) [Li *et al.* (2009)]. However, the cross-slot flow offers the advantage of distancing the point at which extensional flow is measured from any uncontrolled surfaces.

Various constitutive equations have been examined previously in a cross-slot geometry. Bogaerds *et al.* (1999) showed that the Giesekus and PTT models fail to predict downstream principal stresses in cross-slot geometry for polymer solutions due to a failure of capturing extensional stresses. Abedijaberi *et al.* (2009) investigated the flow of LDPE branched polymer melts in a lubricated cross-slot channel by experiments and flow simulations. In this paper, we use the multi-mode Pompom equations [McLeish and Larson (1998); Inkson *et al.* (1999); Blackwell *et al.* (2000), Lee *et al.* (2001)], which has been shown be capable of capturing the quantitative non-linear rheology of LDPE and other long chain branched melts. It is the purpose of this paper to develop "cross-slot extensional rheometry" (CSER) into a quantitative measure of elongational steady states of LCB melts, assisted by accurate flow-modeling, and to apply it to the challenge of the steady-state extensional stress in this class of materials.

II. EXPERIMENTAL MEASUREMENTS

A. Materials

A range of commercial polyethylenes from various production processes and with different branching structure and molar mass distributions has been chosen for this study. The polymers comprise high-density polyethylenes obtained from metallocene catalysis with varying amounts of long-chain branches [Woods-Adams and Costeux (2001)] and commercial low-density polyethylenes from tubular reactor polymerization. Molecular characterization was carried out by combined high temperature size exclusion chromatography (HT-SEC) with appended multi-angle laser light scattering (MALLS), which is a direct method for the determination of absolute molecular weights M_{LS} and square of the radius of gyration $\langle R_g^2 \rangle_z$.

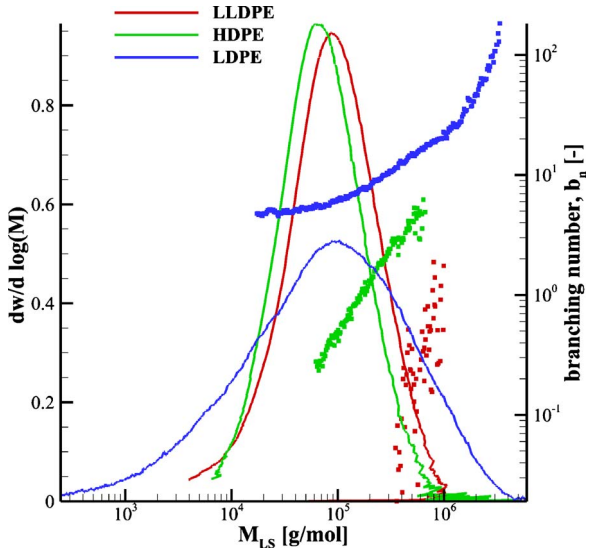

FIG. 1. Molar mass distribution and number of branches from SEC-MALLS (for LLDPE1, HDPE3, and LDPE3).

The molar mass dependence of the radius of gyration $\langle R_g \rangle(M)$ or hydrodynamic radius, respectively, was used to analyze the branching structure of branched polymers. The value of M is typically higher for branched polymers compared to linear polymers at a given elution time. The number of branches can be estimated from $\langle R_g \rangle(M)$ according to the Zimm–Stockmayer theory [Zimm and Stockmayer (1949)].

The HDPE samples all have a very similar molecular weight distribution and class of branching topology, but have an increasing number of branches according to the polymerization process. These samples were successfully described by *ab initio* theoretical modeling capturing the linear rheological response [Das *et al.* (2006)]. The LDPE3 sample (Dow 150R) has already been investigated in previous processing and flow prediction studies by Hassell *et al.* (2008) and Martyn *et al.* (2009). The LDPEs have a broad molecular weight distribution and distinct high molecular weight tail in comparison to the HDPE samples (see Fig. 1). The different distribution widths are reflected by the polydispersity M_w/M_n listed in Table I. The molecular weight averages M_w and branching structures determine the zero-shear-rate viscosities η_0 (see Table I). The values for the HDPE and LLDPE series and LDPE3 are consistent with previous studies [Wood-Adams and Dealy (2000); Crosby *et al.* (2002); den Doelder *et al.* (2005); and Hassell *et al.* (2008)].

B. Experimental rheometry

The pellet grade materials were characterized in both shear and uniaxial extensions at the same temperature as the subsequent cross-slot experiments. Shear flow experiments were conducted with an ARES rheometer (Advanced Rheometric Expansion System, Rheometric Scientific) in order to obtain the linear rheological and non-linear shear flow behaviors as well the corresponding spectra. The non-linear flow behavior in uniaxial elongation was characterized using the uniaxial stretching device Sentmanat Elongational Rheometer (SER) (Xpansion Instruments) attached to the ARES rheometer [Sentmanat (2004)]. Specimen dimensions at test temperature were corrected to consider thermal

TABLE I. Material properties of polyethylenes investigated. The values for the HDPE and LLDPE series and LDPE3 are consistent with previous studies [Wood-Adams and Dealy (2000), Crosby *et al.* (2002), den Doelder *et al.* (2005), and Hassell *et al.* (2008)].

Sample	Code	M_W (kg/mol)	M_W/M_N	T (°C)	η_0 (kPa s)	$\bar{\tau}_b$ (s)
Tubular LDPE1	1800S	146	7	140	2	1.38
Tubular LDPE2	1840H	240	9	150	51	50
Tubular LDPE3	Dow150R	242	11	160	368	428
LCB-met. HDPE1	HDB1	77	2.1	155	11	5.6
LCB-met. HDPE2	HDB2	82	2.1	155	27	14.8
LCB-met. HDPE3	HDB6	68	2.2	155	50	28
Lin-met. LLDPE1	CM1	104	2.1	155	7.9	1.09
LCB-met. LLDPE2	CM2	92	2.2	155	32	16.3
LCB-met. LLDPE3	CM3	84	2.2	155	35	18

expansion by using the room-temperature density and the thermal expansion coefficient of the samples. All of the rheological experiments were carried out under a nitrogen atmosphere, and further rheological tests to assess the thermal stability of the samples were conducted to ensure that the molar mass distribution and the molecular structure did not change during the experiments. A sufficient thermal stability of at least 10^4 s was found for all materials.

The time-dependent tensile stress growth coefficient $\eta_E^+(t,\dot{\varepsilon})$ is determined as

$$\eta_E^+(t,\dot{\varepsilon}) = \frac{\sigma^+(t,\dot{\varepsilon})}{\dot{\varepsilon}}, \tag{2.1}$$

where $\dot{\varepsilon}$ is the imposed extension rate.

The linear rheological behavior of the samples with reptation times larger than 300 s is determined from a combination of frequency sweeps and creep recovery tests, thus reaching time scales of 10^4 s. A very good superposition of the resulting moduli is found for the overlap of dynamic data from creep and creep recovery tests.

C. Cross-slot flow experiments

For the complex flow experiments we employed a Cambridge multi-pass rheometer (MPR), which is a dual piston capillary-type rheometer designed for small quantities of material [Mackley *et al.* (1995)]. The instrument was used with a cross-slot insert and enables simultaneous and time-resolved pressure and optical measurements as reported previously in detail by Coventry and Mackley (2008) and used for a number of different polymer melt flow studies, [e.g., Hassell and Mackley (2007); Hassell and Mackley (2009); Hassell *et al.* (2009)]. The birefringence was measured using a circularly polarized monochromatic light beam of 514 nm using polarizers and quarter waveplates either side of the optical test section which contained stress free quartz windows. The stress-induced birefringence patterns were captured by a digital video camera [Collis and Mackley (2005)]. From the top and bottom reservoirs, the polymer material is driven in opposite directions along two perpendicular channels by pistons at a controlled rate and with equal pressure through the midsection cube into two horizontal side channels with slave pistons (Fig. 2(a)). Thereby, the material is maintained within the MPR and can be forced back by nitrogen pressure through the cross-slot insert into the top and bottom reservoirs for subsequent runs. The cross-slot geometry insert used in this study consists of four

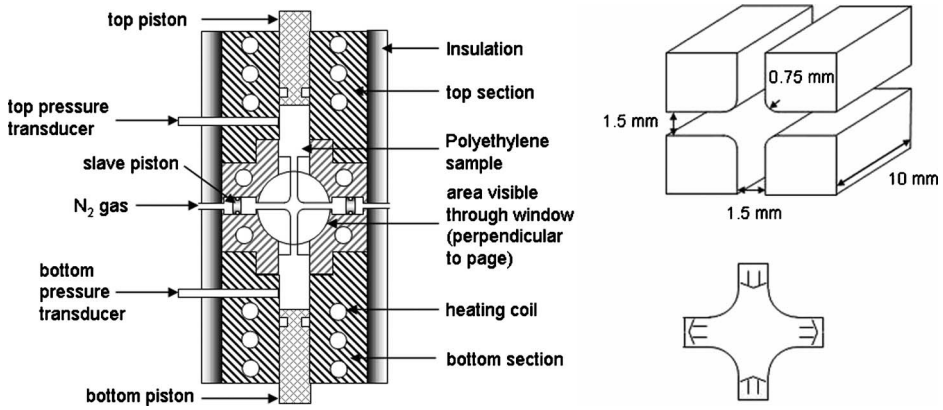

FIG. 2. (a) Schematic outlining the MPR core and (b) the dimensions and flow direction for the cross-slot geometry insert as used in the mid-section of the MPR. The associated flow directions are indicated by arrows.

perpendicular, intersecting coplanar channels with a depth of 10 mm and aspect ratio of about 7 [Fig. 2(b)]. Full three dimensional flow simulations and experiments for linear polystyrene in this geometry [Lord *et al.* (2010)] have demonstrated that this aspect ratio is sufficiently large for the flow to be approximated as two-dimensional, confirming previous simulation studies of Clemeur *et al.* (2004), although an increase in branching has been found to enhance the three-dimensional nature of the flow into a contraction [Hertel *et al.* (2008)]. The two streams, which are pumped into the cross-slot channel, generate a pure and controllable elongational deformation around the stagnation point and along the inlet-outlet symmetry plane, but essentially simple shear near the outer walls, e.g., Coventry and Mackley (2008) and Hassell *et al.* (2008).

At steady state at the stagnation point, a molecule experiences a constant extension rate $\dot{\varepsilon}$. The value of $\dot{\varepsilon}$ can be estimated from the flow of a Newtonian fluid in this geometry, giving a relationship between the extension rate and the piston speed, V_p, of the form

$$\dot{\varepsilon}_C = AV_p, \tag{2.2}$$

where A scales as the reciprocal of the channel width. We shall denote $\dot{\varepsilon}_i$ as the strain-rate at the stagnation point for a Newtonian fluid at this piston speed. However, the exact numerical value of A depends on the constitutive behavior of the melt throughout the flow. For this, we shall use self consistent flow simulations to determine the stagnation point extension rate for each experiment. The steady-state elongational viscosity η_P^+ is calculated from the time-independent tensile stress σ, which is determined from the number of fringes, and the steady-state strain rate $\dot{\varepsilon}_C$ as determined from the flow field:

$$\eta_P^+ = \frac{\sigma_{std}}{\dot{\varepsilon}_C}, \tag{2.3}$$

where $\sigma_{std}=(\sigma_{xx}-\sigma_{yy})$ is the principal stress difference between the extensional x and compressional y axes. Stress induced birefringence was used to observe the principal stress difference (PSD) during flow. The retardation of light between the two principal axes within the polymer, represented as the difference in the refractive indices, is given by the stress- optical rule (SOR) as

$$\Delta n = \mathrm{SOC}\sqrt{(\sigma_{xx}-\sigma_{yy})^2 + 4\sigma_{xy}^2}, \tag{2.4}$$

where the stress-optical coefficient (SOC) is given in units of Pa^{-1}. This relation has been found to be a linear function for stresses up to about 1 MPa in case of low-density polyethylenes [Kotaka *et al.* (1997); Koyama and Ishizuka (1989)] as well as polystyrenes [Luap *et al.* (2006); Venerus and Zhu (1999)]. For the work presented in the subsequent sections, the stresses are below this limit and therefore, the SOR is expected to be valid. Stress-optical coefficients taken from Hassell *et al.* (2008) were used for the experimental and computational work, which is in quantitative agreement with the range given in the literature for polyethylene of $(1.2–2.4)\times 10^{-9}$ Pa^{-1} [Macosko (1994)]. According to the theory of rubber elasticity and also experiments, the stress-optical coefficient is only weakly dependent on temperature [Koyama and Ishizuka (1989)].

III. NUMERICAL FLOW SIMULATIONS

A. The Pompom model

In order to determine the extension rate at the stagnation point, $\dot{\varepsilon}_C$, numerical simulations of the cross-slot flow were performed using a multi-mode version of the Pompom model [McLeish (1988, 2002); McLeish and Larson (1998)].

In the multi-mode Pompom model, the extra stress tensor is formed from the sum of contributions from different relaxation modes [Inkson *et al.* (1999)]. The stress contribution from each mode is the product of the corresponding backbone stretch, λ_i, and orientation tensor $\underline{\underline{S}}_i$,

$$\underline{\underline{\sigma}}(t) = \sum_i \underline{\underline{\sigma}}_i = 3\sum_i g_i \lambda_i^2(t)\underline{\underline{S}}_i, \tag{3.1}$$

where g_i is the modulus of the ith mode. Incorporating the flow-induced branch point displacement discussed by Blackwell *et al.* (2000), the non-dimensional backbone stretch $\lambda_i(t)$ evolves as

$$\frac{D\lambda_i(t)}{Dt} = \lambda_i(t)\underline{\underline{K}}:\underline{\underline{S}}_i - \frac{1}{\tau_{s_i}}(\lambda_i(t)-1)e^{\nu_i^*(\lambda_i(t)-1)}, \tag{3.2}$$

but with λ_i constrained below a maximum stretch q_i. Here τ_{si} is the stretch relaxation time, $\nu_i^* = 2/q_i - 1$, and $\underline{\underline{K}}$ is the deformation rate tensor. In the multi-mode model for a complex LCB melt, the number q_i is interpreted as the "priority" of the segments with corresponding relaxation time or mean number of arms on the exterior of the LCB molecule connected to it [McLeish (2002)].

The unit orientation tensor $\underline{\underline{S}}_i$ is obtained from an auxiliary tensor $\underline{\underline{A}}$,

$$\underline{\underline{S}}_i = \frac{\underline{\underline{A}}_i}{\mathrm{tr}\,\underline{\underline{A}}_i}, \tag{3.3}$$

where $\mathrm{tr}\,\underline{\underline{A}}_i$ denotes the trace of the auxiliary tensor $\underline{\underline{A}}_i$, and $\underline{\underline{A}}_i$ satisfies an upper convected Maxwell equation:

$$\frac{D\underline{\underline{A}}_i}{Dt} = \underline{\underline{K}}\cdot\underline{\underline{A}}_i + \underline{\underline{A}}_i\cdot\underline{\underline{K}}^T - \frac{1}{\tau_{bi}^*}(\underline{\underline{A}}_i - \underline{\underline{I}}). \tag{3.4}$$

For $\lambda_i \geq 1$, the orientation time τ_{bi}^* is equal to the linear relaxation time τ_{bi} of mode i. However, in a scenario such as a reversing flow where $\lambda_i < 1$, the recovery of the chain

to its original length creates new isotropic tube segments, so that the effective orientation relaxation rate becomes [Lee *et al.* (2001)]

$$\frac{1}{\tau_{bi}^{*}} = \frac{1}{\tau_{bi}} + \frac{\dot{\lambda}_i}{\lambda_i} - \underline{\underline{K}}:\underline{\underline{S}}_i \quad \text{for} \quad \lambda_i < 1. \tag{3.5}$$

Two dimensional calculations of the flow of the Pompom model in the cross-slot geometry were performed using a finite element method to compute strain-rate and PSD. Details of the numerical scheme are given in Tenchev *et al.* (2008); Lord *et al.* (2010). Due to symmetry, only one-quarter of the cross-slot domain was calculated. Upstream we impose fully developed channel flow equivalent to the imposed volume flux. Spatial convergence was checked by comparing solutions obtained on two different meshes of 970 and 2600 nodes. Simulations took up to 48 h on a 1.7 GHz processor depending on mesh refinement and time step interval, which is considerably faster than the moving mesh Eulerian–Lagrangian used in our previous study [Hassell *et al.* (2009)].

Since Eq. (3.4) predicts unlimited stretch of the auxiliary tensor $\underline{\underline{A}}$, a finitely extensible nonlinear elastic modification was made to the relaxation term to limit the trace of $\underline{\underline{A}}$ to 1000. A penalty scheme was used to limit the stretch variable to the range $0 \leq \lambda(t) \leq q$.

B. Choice of parameter values

For each material, dynamic shear data were used to determine the linear viscoelastic behavior of each material from which a 12 mode Maxwell spectrum for g_i and τ_{bi} was obtained. Transient shear and uniaxial extension are then used to determine the nonlinear parameters τ_{si} and q_i. The software used was REPTATE developed as part of the micro-scale polymer processing project (μPP^2) [Ramirez and Likhtman (2007)].

Figure 3 shows the results of this fitting for nine of the materials of Table I. Model parameters are listed in Tables IV–VIII. The shear and elongational viscosity measurements at small deformations reproduce the linear viscoelastic response reasonably well and the resulting visco-elastic envelope is indicated for strain-rates between 0.003 and 30 s^{-1}. The results on the HDPE and the LDPE are consistent with previously reported data for these materials from other researchers, e.g., Das *et al.* (2006); Martyn *et al.* (2009); Wood-Adams and Dealy (2000). However, the absence from most of the experimental data of a clear steady-state in elongation leads to an imprecision in fitting the q_i parameters. In stretching experiments inhomogeneously causes a leveling off or decrease in the elongational viscosity and when the experimental extensional viscosity starts to decrease subsequent data are discarded. Thus, it remains unclear whether a steady-state elongational viscosity has been achieved. A similar behavior has often been reported in literature. For example, Minoshima and White (1986) found ductile failure at small elongational deformation for Ziegler–Natta HDPE with a broad molecular weight distribution. This "masking" of any extension-thinning in sample stretching experiments is one of the motivations for the new methodology described in this paper.

Although these materials have a broad spectrum of relaxation time, a viscosity average relaxation time of the polymer $\bar{\tau}_b$ is defined as

$$\bar{\tau}_b = \frac{\sum_i^N g_i \tau_{bi}^2}{\sum_i^N g_i \tau_{bi}} \tag{3.6}$$

from which we can define an average Weissenberg number as $Wi = \bar{\tau}_b \dot{\varepsilon}_i$.

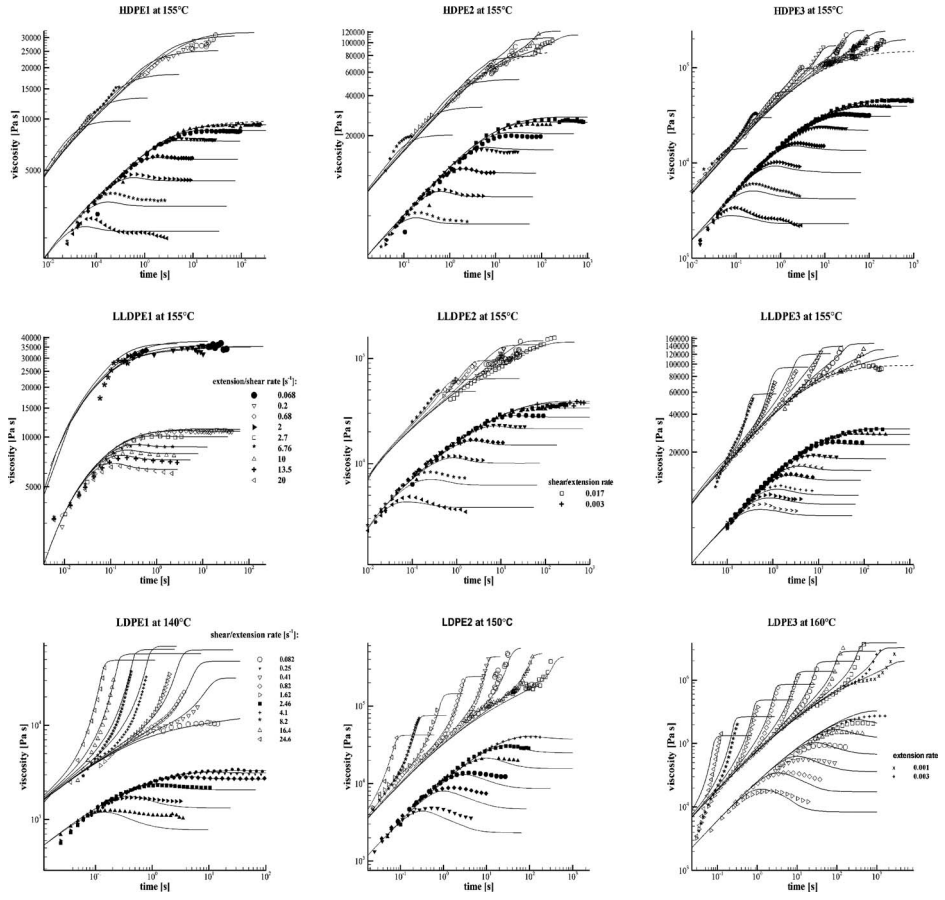

FIG. 3. Time-dependent shear and elongational viscosity η_E from constant strain-rate tests at different strain-rates between 30 and 0.01 s^{-1} for HDPE, LLDPE, and LDPE samples for the temperatures indicated in Table I, ranging from 140 to 160 °C. Symbols are from measurements and the lines are fitted calculations using the Pompom model parameters (see Tables IV–VI). For a particular strain-rate value, identical symbols are used for shear (closed) and elongation (open), which are defined in Table II.

C. Cross-slot flow of a single mode Pompom model

To illustrate how the separate effects of orientation and stretch affect the principal stress difference pattern, we consider the case of a single Pompom mode. Since orientation and stretch are characterized by two different relaxation times, there are two separate Weissenberg numbers: the orientation Weissenberg number $Wi_b = \tau_b \dot{\varepsilon}_i$ associated with the relaxation of orientation through reptation and a stretch Weissenberg number $Wi_s = \tau_s \dot{\varepsilon}_i$.

Figure 4(a) shows a case where both $Wi_b, Wi_s \ll 1$ so that the fluid is effectively Newtonian. The principal stress difference has fourfold symmetry due to the upstream-

TABLE II. The symbols used for transient shear and transient uniaxial extension plots in Fig. 3. Other strain-rates are specified in the plots.

Strain/shear rate (s^{-1})	0.01	0.03	0.1	0.3	1.0	3.0	10	30
Symbol	□	△	○	▽	◇	▷	*	◁

TABLE III. Values of average upstream velocity and stagnation point strain-rates, $\dot{\varepsilon}_i$.

Piston speed (mm s^{-1})	0.044	0.088	0.22	0.44	0.88
Average upstream velocity (mm s^{-1})	0.23	0.46	1.15	2.30	4.61
Strain rate (s^{-1})	0.35	0.70	1.75	3.48	6.95

downstream symmetry of Stokes flow. In Fig. 4(b), the flow is orientating but not stretching, i.e., $W_{ib} > 1, W_{is} < 1$, which is typical of (polydisperse) linear polymer melts such as HDPE. Finally, Fig. 4(c) shows a flow that is both orientating and stretching, i.e., $W_{ib}, W_{is} > 1$. In this case, the PSD pattern is determined by priority branching number q, which controls the maximum value which the backbone stretch can reach. High branching numbers produce very narrow and extended birefringence lines along the central outflow axis.

The presence of high levels of molecular stretch and hence stress along the outflow center line can affect the fluid velocity and hence the strain rate at the stagnation point. The strain-rate, $\dot{\varepsilon}_i$, used in the definition of the Weissenberg number is the initial strain rate when the stress is Newtonian, while the true steady-state strain-rate is denoted by $\dot{\varepsilon}_C$. In Fig. 5, we show how the form of the x component of the fluid velocity varies for three choices of q.

For high values of q, the presence of high stresses along the downstream center line slows down the velocity and therefore $\dot{\varepsilon}_C$ is lower than for the equivalent Newtonian fluid [Fig. 5(d)]. However, for low values of q, we find the opposite effect [Fig. 5(b)]. The stretch parameter λ reaches its maximum value of q so that the stress no longer increases with strain. This loss of strain-hardening causes the velocity near the stagnation point to speed up. At intermediate values of q, the x velocity becomes independent of y near the stagnation point [Fig. 5(c)].

While these effects on the velocity are exaggerated in single mode model, the degree of strain-hardening in multimode model can still cause changes of up to 20% in the steady-state strain-rate compared to its initial (Newtonian) value $\dot{\varepsilon}_i$. Figure 6 show how

TABLE IV. A list of Pompom parameters used throughout this study.

	LLDPE1 at 155 °C—12 modes				LLDPE2 at 155 °C—13 modes			
Mode, i	g_i (Pa)	$\tau_{b,i}$ (s)	$\tau_{b,i}/\tau_{s,i}$	q_i	g_i (Pa)	$\tau_{b,i}$ (s)	$\tau_{b,i}/\tau_{s,i}$	q_i
1	324 041.441 3	0.005 011 872	⋯	1	210 295.427 5	0.005 862 595	⋯	1
2	137 478.130 4	0.010 873 357	⋯	1	88 330.357 78	0.013 205 328	⋯	1
3	72 139.788 91	0.023 589 964	⋯	1	35 687.223 78	0.029 744 622	⋯	1
4	39 856.792 8	0.051 178 896	⋯	1	24 142.480 28	0.066 998 909	⋯	1
5	16 198.810 14	0.111 033 632	⋯	1	12 841.070 63	0.150 913 122	⋯	1
6	5 774.949 113	0.240 889 673	⋯	1	7 587.825 93	0.339 927 483	⋯	1
7	914.271 068 5	0.522 614 937	⋯	1	5 056.597 314	0.765 676 912	⋯	1
8	312.033 447 7	1.133 823 501	⋯	1	2 106.607 232	1.724 665 298	4	2
9	54.633 161 23	2.459 852 639	⋯	1	1 219.447 935	3.884 759 153	4	3
10	25.450 939 77	5.336 699 231	⋯	1	683.099 263 9	8.750 308 648	5	3
11	14.577 050 93	11.578 075 14	⋯	1	243.090 446 8	19.709 819 43	5	3
12	13.297 715 66	25.118 864 32	⋯	1	88.269 481 98	44.395 803 35	5	4
13					29.155 224 53	100.000 274 6	5	7

TABLE V. A list of Pompom parameters used throughout this study.

	LLDPE3 at 155 °C—12 modes				HDPE1 at 155 °C—12 modes			
Mode, i	g_i (Pa)	$\tau_{b,i}$ (s)	$\tau_{b,i}/\tau_{s,i}$	q_i	g_i (Pa)	$\tau_{b,i}$ (s)	$\tau_{b,i}/\tau_{s,i}$	q_i
1	247 540.174 4	0.006 309 573	⋯	1	433 472.679 4	0.001	⋯	1
2	41 955.240 14	0.018 738 174	⋯	1	122 600.654 5	0.002 848 036	⋯	1
3	20 339.876 91	0.055 648 639	⋯	1	73 615.908 38	0.008 111 308	⋯	1
4	12 961.309 29	0.165 265 354	⋯	1	30 072.135 16	0.023 101 297	⋯	1
5	6 872.941 193	0.490 805 127	⋯	1	11 178.246 7	0.065 793 322	⋯	1
6	3 841.269 813	1.457 593 301	⋯	1	5 265.635 789	0.187 381 742	⋯	1
7	1 430.958 955	4.328 761 281	6	8	2 749.195 783	0.533 669 923	⋯	1
8	347.444 303 1	12.855 557 32	6	8	1 143.611 026	1.519 911 083	⋯	1
9	134.989 038	38.178 440 26	6	8	338.296 801 4	4.328 761 281	⋯	1
10	12.820 132 25	113.382 350 1	4	12	55.188 494 16	12.328 467 39	⋯	1
11	0.718 380 772	336.722 957 5	4	20	7.948 397 277	35.111 917 34	⋯	1
12	0.041 555 617	1000	4	25	2.616 843 93	100	1	2

the fluid velocity along the outflow center line changes as the stresses build up. Near the stagnation point, the velocity increases relative to the Newtonian solution and passes through a maximum before decreasing to a lower steady value.

IV. RESULTS AND DISCUSSION

A. Rheological behavior in the cross-slot flow

One of the main objectives of this work is to compare the elongational behavior found in the planar extensional flow in the cross-slot geometry with the transient uniaxial extensional rheology measured from the SER. Of course, the two experiments measure different extensional flow types and for Newtonian fluids there is a factor 4/3 difference between the planar and uniaxial extensional viscosities. However, this difference diminishes in non-linear response at high Weissenberg numbers where little difference is found

TABLE VI. A list of Pompom parameters used throughout this study.

	HDPE2 at 155 °C—12 modes				HDPE3 (a) at 155 °C—12 modes			
Mode, i	g_i (Pa)	$\tau_{b,i}$ (s)	$\tau_{b,i}/\tau_{s,i}$	q_i	g_i (Pa)	$\tau_{b,i}$ (s)	$\tau_{b,i}/\tau_{s,i}$	q_i
1	413 109.316 2	0.001	⋯	1	219 226.254	0.000 848 266	⋯	1
2	152 056.861	0.002 848 036	⋯	1	179 387.352 1	0.002 801 581	⋯	1
3	91 389.621 61	0.008 111 308	⋯	1	37 873.852 47	0.009 252 826	⋯	1
4	41 271.545 17	0.023 101 297	⋯	1	32 981.422 78	0.030 559 456	⋯	1
5	16 646.576 19	0.065 793 322	⋯	1	18 896.902 18	0.100 929 202	⋯	1
6	9 659.771 983	0.187 381 742	⋯	1	11 820.399 86	0.333 340 482	⋯	1
7	5 507.878 787	0.533 669 923	⋯	1	6 053.396 303	1.100 928 915	⋯	1
8	2 876.600 869	1.519 911 083	⋯	1	2 767.032 716	3.636 055 443	9	3
9	1 296.608 041	4.328 761 281	10	1.3	840.574 526 1	12.008 858 16	9	3
10	417.051 569 6	12.328 467 39	9	1.3	224.024 049	39.661 846 92	3	5
11	75.965 745 43	35.111 917 34	8	2	26.774 598 65	130.991 812 9	2	8
12	23.022 632 92	100	1.2	5	1.945 588 697	432.628 744 5	7	20

TABLE VII. A list of Pompom parameters used throughout this study.

Mode, i	LDPE1 at 140 °C—12 modes				LDPE2 at 150 °C—12 modes			
	g_i (Pa)	$\tau_{b,i}$ (s)	$\tau_{b,i}/\tau_{s,i}$	q_i	g_i (Pa)	$\tau_{b,i}$ (s)	$\tau_{b,i}/\tau_{s,i}$	q_i
1	42 020.864 12	0.005 011 872	⋯	1	64 373.252 86	0.003 162 278	⋯	1
2	9 803.492 514	0.01	⋯	1	37 846.433 03	0.01	⋯	1
3	7 989.028 802	0.019 952 623	⋯	1	13 408.433 18	0.031 622 777	1.3	4
4	5 305.426 687	0.039 810 717	⋯	1	14 121.939 55	0.1	4.7	5
5	3 444.057 023	0.079 432 823	2.2	9	7 155.575 024	0.316 227 766	5	5
6	2 448.643 774	0.158 489 319	2.2	10	4 417.122 368	1	5	6
7	1 209.928 886	0.316 227 766	2.2	11	2 191.354 634	3.162 277 66	5	7
8	768.726 368 7	0.630 957 344	2.2	12	1 034.367 414	10	5	8
9	346.387 748 1	1.258 925 412	2.2	14	404.688 671 7	31.622 776 6	2.6	9
10	99.166 548 91	2.511 886 432	2	18	88.189 190 19	100	2.6	14
11	36.459 217 33	5.011 872 336	2.1	22	7.910 956 212	316.227 766	1	15
12	18.996 958 63	10	2.5	25	0.340 160 159	1 000	1	16

between results of uniaxial and planar extension [e.g., Inkson *et al.* (1999); Laun and Schuch (1989)]. The Pompom constitutive model captures this diminishing effect and in the limit of high strain-rate gives the same steady extensional viscosity for both flow types [Inkson *et al.* (1999)]. At high Weissenberg numbers, the tube segments align with the direction of extension, so that $\underline{\underline{K}}:\underline{S}_i \rightarrow \dot{\varepsilon}$. Consequently, the stretch equation becomes the same for both flow types giving the same extensional viscosity for both flow types.

In order to determine the steady-state viscosity from cross-slot rheometry, it is important to achieve a steady-state stress profile. Even for the highly branched LDPE, with long relaxation times, the birefringence patterns equilibrate, with no further change, within the experimental time and strain window of about 6 Hencky strain units, and thus indicating a steady-state flow condition. This steady state was observed to have been reached well before the end of the experimental time frame for all the materials in our

TABLE VIII. A list of Pompom parameters used throughout this study.

Mode, i	LDPE3 at 160 °C—12 modes			
	g_i (Pa)	$\tau_{b,i}$ (s)	$\tau_{b,i}/\tau_{s,i}$	q_i
1	640 715.489 88	0.003 981 072	⋯	1
2	45 406.567 05	0.012 855 557	⋯	1
3	23 491.123 46	0.041 512 78	⋯	1
4	19 983.818 26	0.134 051 824	⋯	1
5	12 836.590 43	0.432 876 128	4	7
6	8 565.188 481	1.397 830 607	5	7
7	5 152.392 951	4.513 832 66	5	7
8	2 934.186 895	14.575 933 01	5	7
9	1 436.929 912	47.068 165 6	5	8
10	635.072 026 9	151.991 108 3	5	8
11	176.198 302 5	490.805 127 2	3.5	10
12	45.964 757 89	1 584.893 192	2.3	12

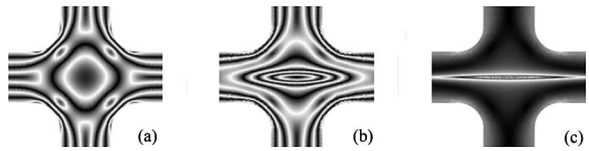

FIG. 4. Qualitative comparison of the predicted shape of the PSD for different flow Weissenberg number regimes for a single Pompom mode (with a solvent mode weighted at 10%): (a) slow flow, (b) orientating but non-stretching flow, and (c) stretching flow.

study. These visual observations of the flow suggest that the residence times and total strains are sufficient to reach a steady-state in transient rheology. The time dependence of the stress profile has been discussed in more detail by Hassell *et al.* (2008).

The intensity patterns of the birefringence can be used to determine the principle stress difference in steady-state extensional flow by measuring the (fractional) fringe number at the flow stagnation point (see Fig. 7 for an example of the fringe counting technique). Figure 8 displays this recorded "raw" data as a function of the flow rate as denoted by the piston speed. The extension rate at the SP can then be calculated from the finite element

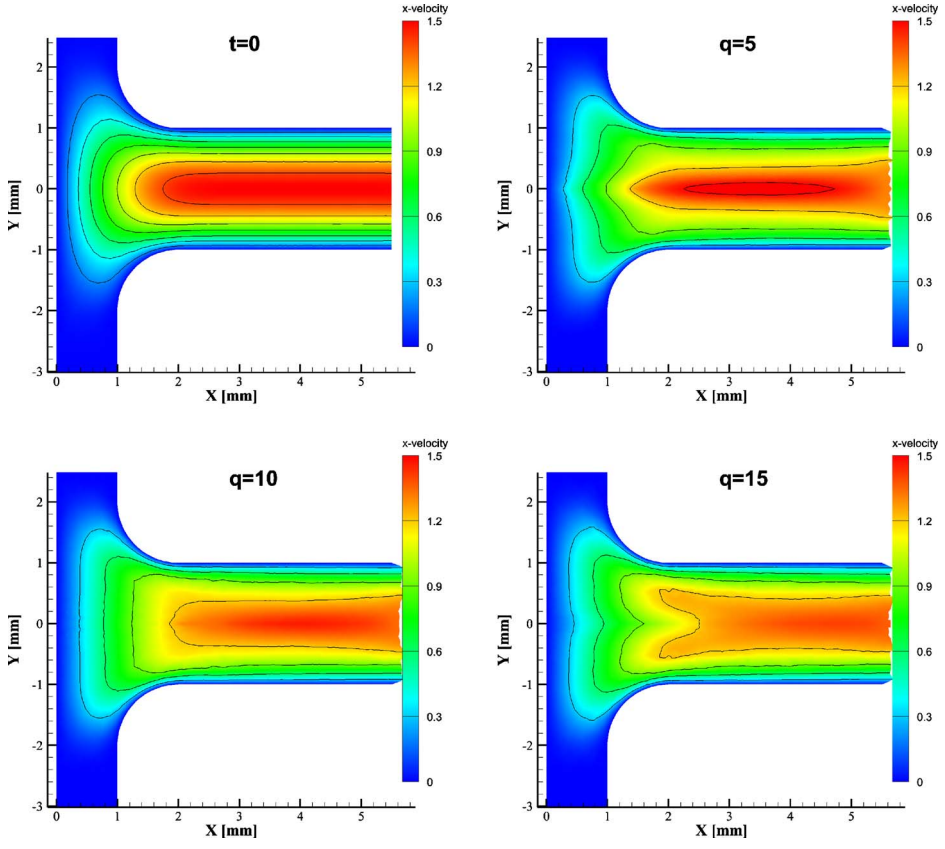

FIG. 5. Contour plots of the x velocity component in the right hand part of the cross-slot: (a) the initial Stokes solution, (b) $q=5$, the velocity near the stagnation point speeds up; (c) $q=10$; d) for large values of $q=15$ the large stretch gradient slows the flow down. Parameters chosen were $G=0.9$, $\tau_b=10$, and $\tau_s=10$ with varying q, this gives an initial Weissenberg number of 10 for both stretch and orientation

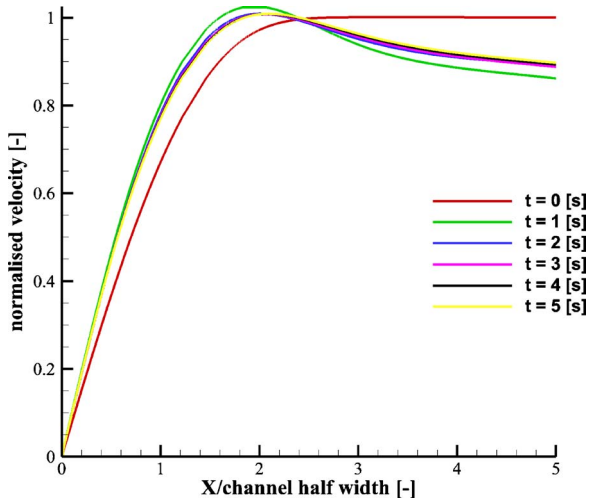

FIG. 6. A comparison of the velocity profile along the downstream symmetry line for the simulated HDPE3 Pompom spectrum as a function of time. Near the stagnation point the velocity increases where the Pompom modes are fully stretched leading to an overshoot in the velocity downstream.

simulations where a transient flow with constant velocity input flux is specified. In Table III, the Stokes strain rate from each piston speed is detailed with corresponding velocity flux condition used in the numerical solutions. The lower limit for the determination of tensile stresses from birefringence is given by the necessary minimum of at least half an established fringe. The resolution for the stress increases significantly with a growing number of fringes since an error of the order of one fringe becomes less pronounced for a higher number of fringes. Toward higher piston speeds, the spatial resolution of the optical equipment limits the maximum number of fringes, which can be distinguished in the 1.5 mm wide cross- slot gap to about 40 fringes, with a possible error of ± 3 fringes due to increasing fringe density.

In Figs. 9–11, the black and white fringes from stress-induced birefringence (photographs in the left part) are compared to the PSD intensity profiles from simulations (color images in the right part) with the PSD level increases from blue to red. To enable a direct comparison, black contour lines are drawn to coincide with the dark experimental birefringence contours with SOC taken from Hassell *et al.* (2008). The similarity of both

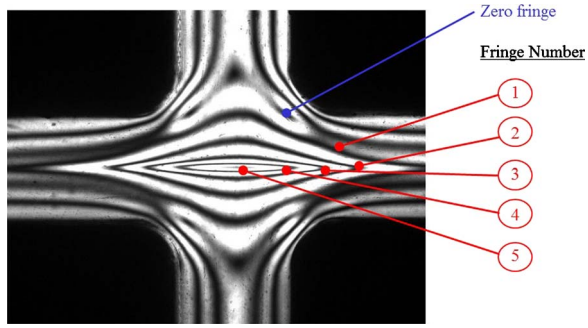

FIG. 7. An example of fringe counting for HDPE2 with an extension rate of $\dot{\varepsilon}_C = 1.9$ in Stokes flow. The example show five fringes each carrying 22 kPa of stress.

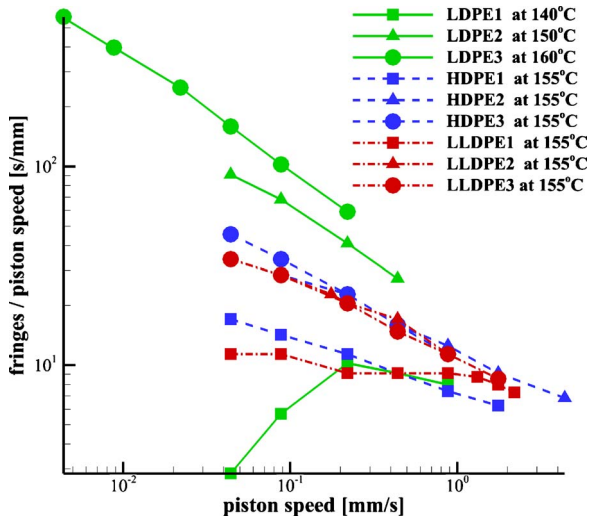

FIG. 8. Number of fringes at the SP divided by piston speed as a function of piston speed for the LLDPE, HDPE, and LDPE samples investigated at conditions indicated in Figs. 9–11.

fringe patterns demonstrates a superficially good agreement for both the stress level and distribution for each material as a function of velocity flux with the initial strain rate shown. Of course, close to the outflow center line none of the simulations captures the W-cusp phenomena, however, away from this region the overall shape is generally predicted well.

The flow-rates and material specific average relaxation times are given so that the particular Weissenberg numbers can be estimated for a particular flow condition. However, these numbers can only give an average since all materials have a relatively wide range of relaxation times due to the width of the molar-mass distribution and also the heterogeneity of the long-chain branching structure. For small Weissenberg numbers, the symmetric PSD patterns indicate a Newtonian behavior and only a small number of fringes for most materials, e.g., the low viscosity samples LLDPE1 and HDPE1. However, in the most extreme case of LDPE3 with a long tail of relaxation times, a non-symmetric PSD arises even at mean Weissenberg numbers less the unity [see Hassell *et al.* (2008)]. With increasing Weissenberg number, the flow birefringence or PSD pattern become increasingly asymmetric due the material memory and strain history effects. Around the stagnation point, highly localized central fringes [see Coventry and Mackley (2008); Verbeeten *et al.* (2001)] and double cusping (W-cusps) of the fringes occur along the outlet centerline for some materials. The latter effect has also been observed for other highly branched materials [Hassell and Mackley (2009); Soulages *et al.* (2008)] and been investigated in more detail in Hassell *et al.* (2009). This effect is not captured by the Pompom model.

B. Steady-state elongational viscosity from stagnation point analysis

As outlined in the sections above, the steady-state elongational viscosity can be determined from the steady-state stress and strain rate at the central cross-slot stagnation point by using the number of fringes to determine the stress difference and the calculated velocity field to find the strain-rate at the stagnation point.

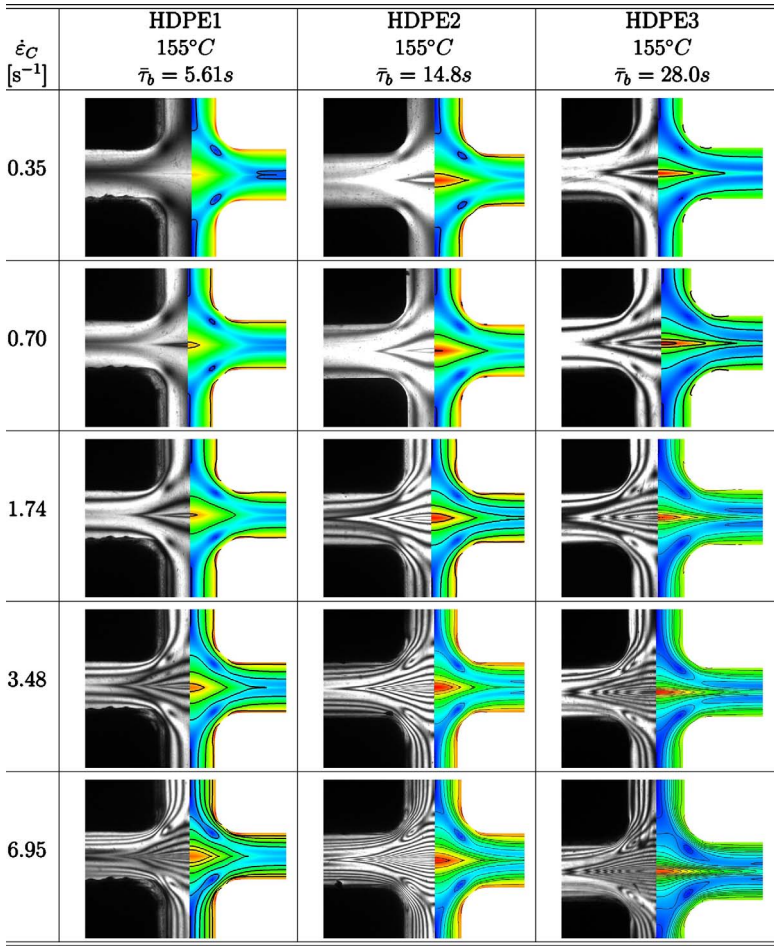

FIG. 9. Comparison between the experimentally observed flow-induced stress birefringence patterns for the HDPE series at different strain-rates with computed values of the principal stress difference shown with a contour interval of 22 kPa for all materials.

The results from the combination of birefringence analysis and flow-rate predictions are presented in Figs. 14–16, in terms of steady-state extensional viscosity as a function of extension rate. Also plotted are the maximum values of the stress obtained in the SER extensional experiments performed on the same samples, assuming that these values are attained at the onset of plateau stress. As noted above, in comparing the SER and cross-slot (CSER) data, account must be taken that two experiments measure different extensional flow types. To show the likely extent of this difference, the Pompom predictions for both uniaxial and planar extensions are shown in Figs. 14–16.

To establish the precision of viscosity measurements from the CSER, the various sources of error must be analyzed. Three values are needed to produce a data point, namely, the number of fringes, the SOC and the strain-rate. The fringe count has a minimum error of half a fringe, which provides the biggest errors at small fringe numbers, i.e., when less than two fringes are visible. At high stress values, typically when the total number of fringes exceeds 15, it becomes difficult to determine the exact number of fringes at the SP due to fringe density there. However, in these cases, errors of ± 3 fringes

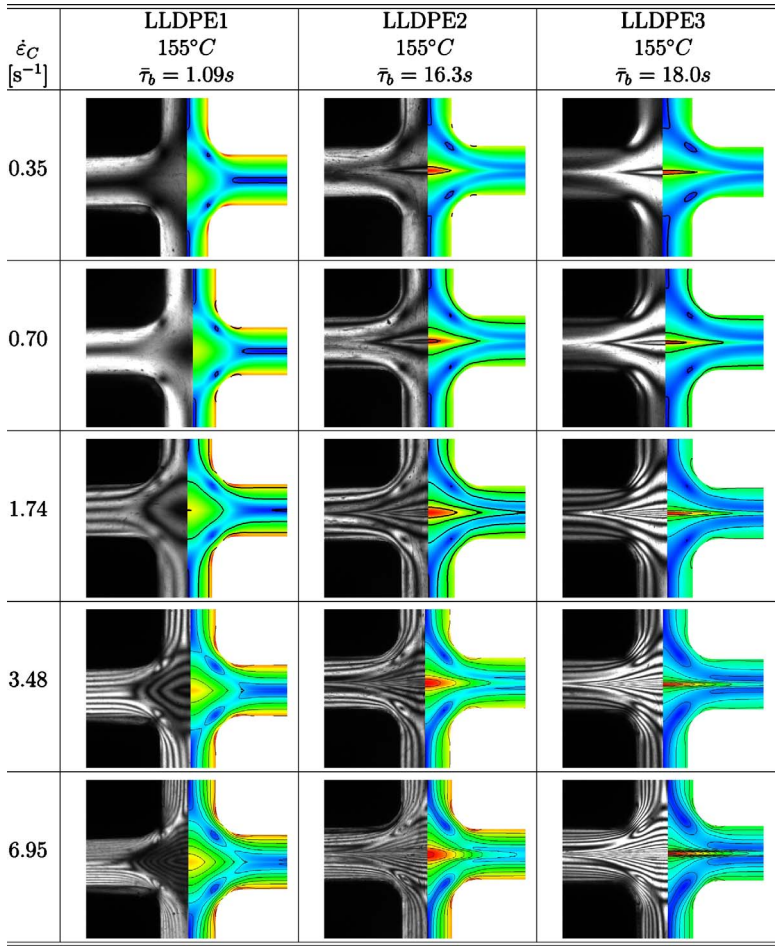

FIG. 10. Comparison between the experimentally observed flow-induced stress birefringence patterns for the LLDPE series at different strain-rates with computed values of the principal stress difference shown with a contour interval of 40 kPa for all materials.

have little visible effect on the viscosity curves in Figs. 14–16, but this does prevent us for analyzing higher flow-rates as we can no longer count the fringes with sufficient certainty. For each fringe to carry a fixed stress contribution, the linear stress-optical relation must be valid with a well defined SOC. For this work, a SOC of 2.34×10^{-9} Pa^{-1}, which is equivalent to 22kPa of stress per fringe is used for the HDPEs, 2.19×10^{-9} Pa^{-1} equivalent to 24.5 kPa of stress per fringe for the LDPEs, and a SOC of 1.29×10^{-9} Pa^{-1} giving 40 kPa of stress per fringe for the LLDPEs. This agrees with previous experimental measures of the SOC using the MPR [Coventry (2006); Hassell *et al.* (2008)] and fall within literature range of $(1.2–2.4) \times 10^{-9}$ Pa^{-1} for polyethylene [Macosko (1994)]. The total error for various materials is summarized in Fig. 12 where the largest error appears if only one fringe is present.

To define the viscosity, the simulated strain rate is used, which can vary from the initial strain rate by up to 20%. As a check on the predictions of simulations, measurements of the fluid velocity along the inlet and outlet center lines were obtained using laser Doppler velocimetry for selected materials and flow rate. Figure 13 shows the compari-

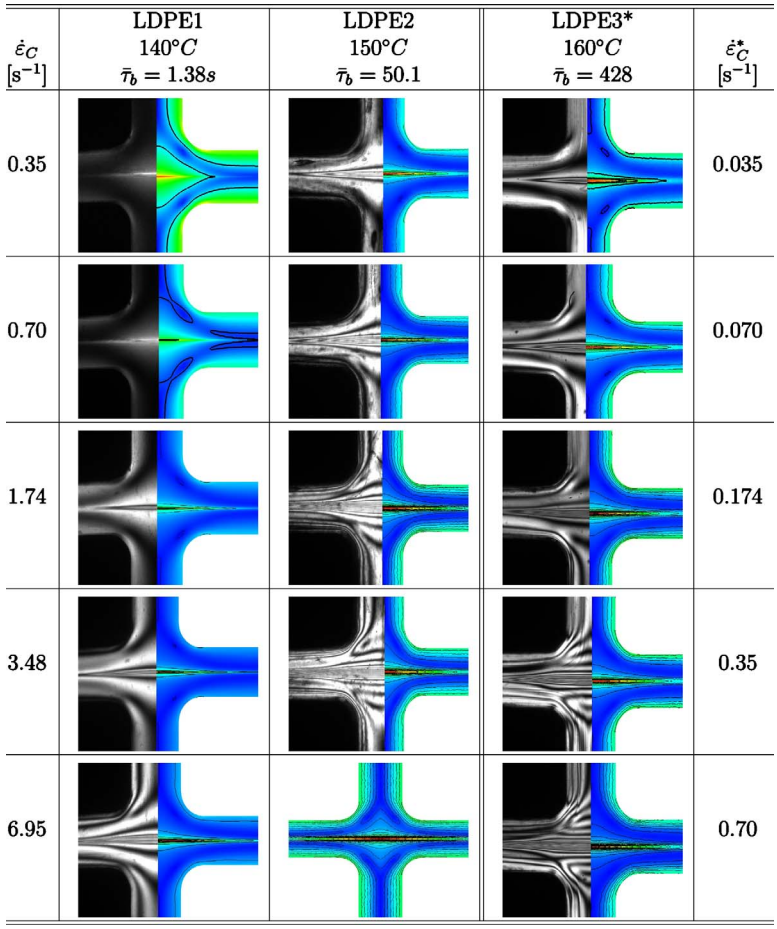

FIG. 11. Comparison between the experimentally observed flow-induced stress birefringence patterns for the LDPE materials at different strain-rates with computed values of the principal stress difference shown with using the same optical constant of 24.5 kPa for the three slowest flow-rates, and for clarity 49 kPa for the two fastest flow-rates. Note, for LDPE3 that the strain-rates are a factor 10 lower than for LDPE1 and LDPE2.

son for HDPE2 and LDPE2 where the flow simulations predict an increase and a decrease, respectively, in the strain-rate compared to a Newtonian fluid. Although the precision of the LDV measurements is limited due to the slow flow-rates, particularly for LDPE2, the results are consistent with the flow simulations. In particular, downstream the HDPE data are higher than the Newtonian values and show an overshoot, whereas the LDPE2 data show a reduction in velocity compared to a Newtonian fluid. Errors in the strain rate will produce a 45 deg translation of the data in Figs. 14–16. Again, errors up to 20% have little visible effect on the extensional viscosity predictions.

For the linear LLDPE1 (Fig. 15) and HDPE1 with little LCB content (Fig. 14), the SER and cross-slot (CSER) extensional viscosity data are in good agreement. The small discrepancy between the data being explained by the difference between uniaxial and planar extensional flow. This is shown by the Pompom predictions agreeing with each flow type for these materials.

The discrepancy between uniaxial and planar extension is smaller for LLDPE2 (Fig. 15) and HDPE2 (Fig. 14), where the data are in the non-linear strain-hardening regime.

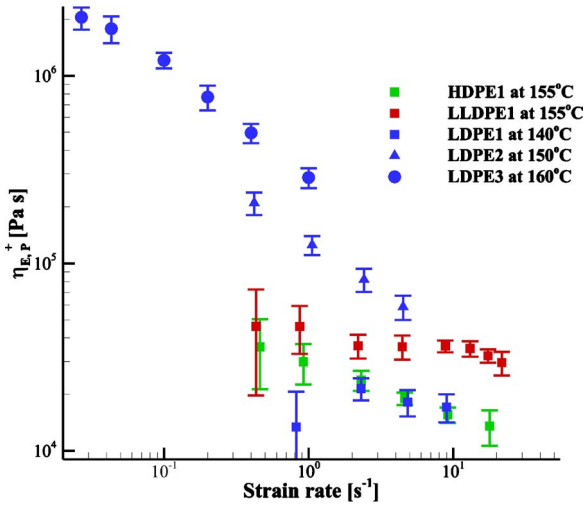

FIG. 12. An example of the error bars for various representative materials. For clarity not all materials are shown as similar viscosity levels produce similar error bars to those materials shown.

For these two materials, the CSER data are slightly higher than the SER data and the Pompom planar prediction. In the cross-slot simulations, the Pompom spectra used for LLDPE2 and HDPE2 did not capture the same number of fringes as seen in the experiments (see Figs. 9 and 10). This suggests the SER stretching experiments do not reach the steady-state plateau and that these materials are more strain hardening than the SER experiments predict. Hence, the CSER steady-state extensional viscosity curve provides a tool for improving rheological testing and parametrizing materials where sample breakup limits transient extensional data.

For the materials HDPE3 (Fig. 14), LDPE2, and LDPE3 (Fig. 16), the CSER data are significantly lower than that of the SER experiments for all measured strain-rates. This

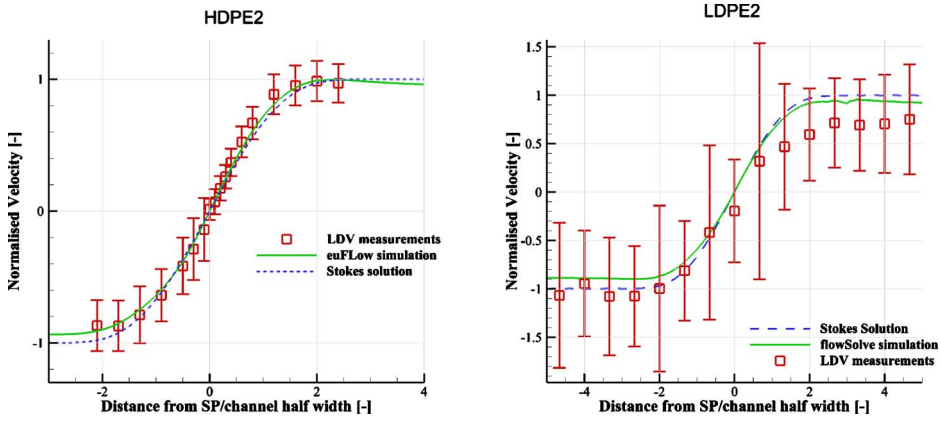

FIG. 13. Experimental results from laser-Doppler velocimetry (symbols) and flow simulations (solid line) for the fluid velocity along the streamline passing through the stagnation point for HDPE2 at 155 °C and LDPE2 at 150 °C. The stagnation point is located at the origin. Negative distances correspond to the y component of velocity along the y axis upstream of the stagnation point (inlet channel) and positive distances to the x velocity component on the x axis downstream of the stagnation point (outlet channel).

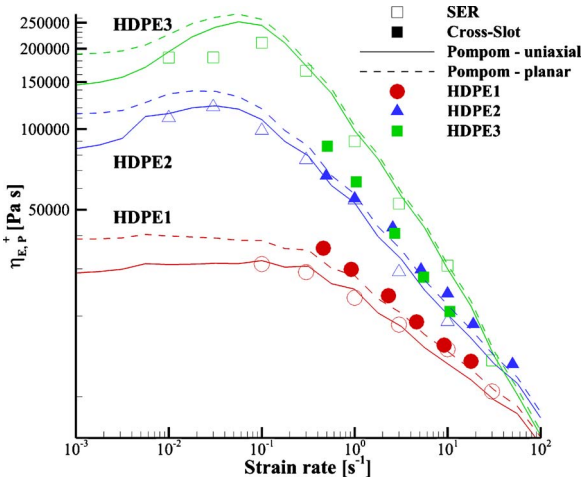

FIG. 14. Elongational viscosity η_E as a function of strain rate from uniaxial (open symbols) and cross-slot experiments (closed symbols) and together with the multimode Pompom predictions for the uniaxial (solid lines) and planar (dashed lines) extensional viscosity for the branched HDPE series.

discrepancy is far larger than the imprecision in the CSER results discussed above. However, all these materials exhibit W-cusps (Figs. 9 and 11). Therefore, since the birefringence along the inlet center line shows the strain history of the material, the appearance of a double cusp indicates an overshoot in the extensional stress with the maximum being larger than the final steady-state value. Overshoot in the transient extensional viscosity of LPDE have been reported by Raible *et al.* (1979) and more recently by Bach *et al.* (2003); Rasmussen *et al.* (2005) using an actively controlled extensional rheometer. This suggests that the W-cusps is a consequence of the constitutive properties of branched materials rather resulting from changes to the velocity gradient.

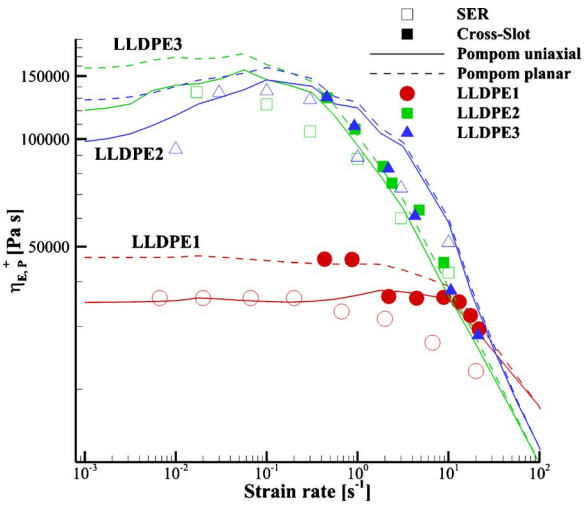

FIG. 15. Elongational viscosity η_E as a function of strain rate from uniaxial (open symbols) and cross-slot experiments (closed symbols) and together with the multimode Pompom predictions for the uniaxial (solid lines) and planar (dashed lines) extensional viscosity for the LLDPE series.

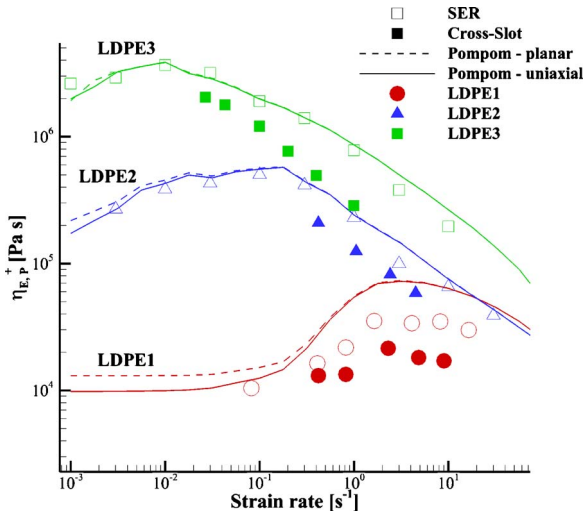

FIG. 16. Elongational viscosity η_E as a function of strain rate from uniaxial (open symbols) and cross-slot experiments (closed symbols) and together with the multimode Pompom predictions for the uniaxial (solid lines) and planar (dashed lines) extensional viscosity for the LDPE series.

The materials LLDPE3 (Fig. 15) and LDPE1 (Fig. 16) show an interesting cross-over between the behaviors observed for the lightly branched materials (LLDPE2 and HDPE2) and the more heavily branched (HDPE3, LDPE2, and LDPE3) materials. At low strain-rates, LDPE1 show a single cusp birefringence pattern (Fig. 11) and SER and CSER measurements agree within precision of the CSER. However, at higher strain-rates, the CSER predicts a lower steady-state value than the SER experiment and W-cusps are present in the FIB pictures. For the material LLDPE3, the extensional viscosity given by the CSER is above that of the SER for the lower strain-rates, but for strain-rates above around 10 s^{-1} the CSER data are below the SER values. However, it is unclear whether the FIB pictures (Fig. 10) exhibit W-cusps at these higher strain-rates as the resolution is not good enough to decipher the tightly packed fringes.

V. CONCLUSIONS

This investigation demonstrates both how the steady-state flow behavior in extensional flow can be determined from cross-slot measurements and also how the presence of long chain branches in the molecular structure affects the stress in an extensional flow. A key assumption in the analysis is that flow is two dimensional, meaning that influence from shear flow at the end walls and secondary flow effects, e.g., vortices, may be neglected. Analyzing polymer melts in a confined reservoir like the cross-slot geometry using the multi-pass rheometer avoids problems created by the presence of free surfaces and localized necking in stretching rheometers. Cross-slot extensional rheometry is complementary to existing extensional rheometers, such as the SER, as it can measure the high strain steady-state limits and does not require the material to be strain-hardening. Furthermore, by analyzing the flow in the inlet channels both shear and elongation properties can be measured simultaneously.

The CSER does have some important limitations. For a given slit depth, there is limited range of extension rates for which fringe counting provides an accurate measurement of the stress. In particular, for highly strain-hardening materials at high strain-rates

the fringe density along the axis becomes too high to count fringes with any confidence. This technique also relies upon the applicability of the stress-optical rule and an accurate determination of the stress-optical coefficient.

In this paper, we used flow computations to determine the stagnation extension rate, in order to take account of any flow field modification. However, for the polymer melts we investigated, we found that the computed extension rate only differs by around 10% from the value found for a Newtonian fluid. Consequently, given the level of other uncertainties with this technique, it would be possible to use the Newtonian extension rate as a reasonable estimate.

For the steady-state elongational viscosity determined in the cross-slot geometry, we generally found a good quantitative agreement with the maximum values determined in uniaxial elongation for materials with a single cusp pattern. However, in some cases, such as HDPE2, the cross-slot data are slightly higher. This may be because sample rupture occurs in the stretching experiments before the steady-state stress is achieved. This discrepancy is reflected in the simulations (fitted to the extensional data from stretching experiments) that predict fewer fringes than are observed in the cross-slot experiments. Using the steady-state extensional viscosity data from the CSER to fit the parameters in the Pompom constitutive theory should improve this prediction. Transient uniaxial data alone are often not sufficient to determine the "priority" branching q-spectrum in the Pompom model uniquely, as there maybe multiple solutions to fitting a multi-mode Pompom spectrum that accounts for limited uniaxial elongational data equally well. However, by using a combination of CSER and sample stretching tests like the SER, the model parameter become much more restricted. For this reason matching, the predicted stress-induced birefringence patterns could become a highly valuable tool in analyzing the branching structure of a polymer melt.

For materials that show W cusps, the CSER gives significantly lower values for the steady-state extensional viscosity than those produced from the Pompom fitting to the SER start-up extensional response. While on its own, this might be thought of as a puzzling short coming of the CSER method, when combined with observations of overshoots in the extensional viscosity of some LCB melts found in actively controlled filament stretching [Bach *et al.* (2003); Rasmussen *et al.* (2005)], it becomes an intriguing indicator of this rarely observed phenomenon. This phenomenon is not reproduced in the simulations with the multimode Pompom models, which suggests that it may be caused by a physical mechanism that is not yet captured in this model. This is an example of new physics that the CSER method points us to and will be the subject of future work.

ACKNOWLEDGMENT

All authors would like to acknowledge funding from EPSRC under the Microscale Polymer Processing Research Project Nos. GR/T11807/01 and GR/T11821/01 and materials from DowChemical and LyondellBasell. Furthermore, we would like to thank Dr. M. Walkley, Dr. R. Tenchev, Dr. D. H. Klein, Dr. J. Embery, Dr. K. Coventry, and Dr. S. Butler for their help and support through many useful discussions.

APPENDIX: POMPOM PARAMETERS

Tables IV–VIII show the parameters used to fit the Pompom constitutive equation (Eqs. (3.1), (3.4), (3.3), (3.2), and (3.5)) to transient shear and extensional data (Fig. 3).

References

Abedijaberi, A., J. Soulages, M. Kröger, and B. Khomami, "Flow of branched polymer melts in a lubricated cross-slot channel: A combined computational and experimental study," Rheol. Acta **48**:0 97–108 (2009).

Bach, A., H. K. Rasmussen, and O. Hassager, "Extensional viscosity for polymer melts measured in the filament stretching rheometer," J. Rheol. **47**(2), 429–441 (2003).

Bent, J., L. R. Hutchings, R. W. Richards, T. Gough, R. Spares, P. D. Coates, I. Grillo, O. G. Harlen, D. J. Read, R. S. Graham, A. E. Likhtman, D. J. Groves, T. M. Nicholson, and T. C. B. McLeish, "Neutron-mapping polymer flow: Scattering, flow visualisation and molecular theory," Science **301**, 1691–1695 (2003).

Blackwell, R. J., O. G. Harlen, and T. C. B. McLeish, "Molecular drag-strain coupling in branched polymer melts," J. Rheol. **44**, 121–136 (2000).

Bogaerds, A. C. B., W. M. H. Verbeeten, G. W. M. Peters, and F. P. T. Baaijens, "3d viscoelastic analysis of a polymer solution in a complex flow," J. Non-Newtonian Fluid Mech. **180**, 413–430 (1999).

Clemeur, N., R. P. G. Rutgers, and B. Debbaut, "Numerical evaluation of three dimensional effects in planar flow birefringence," J. Non-Newtonian Fluid Mech. **123**, 105–120 (2004).

Cogswell, F. N., "Converging flow of polymer melts in extrusion dies," Polym. Eng. Sci. **12**(1), 64–73 (1972).

Collis, M. W., and M. R. Mackley, "The melt processing of monodisperse and polydisperse polystyrene melts within a slit entry and exit flow," J. Non-Newtonian Fluid Mech. **128**(1), 29–41 (2005).

Coventry, K. D., "Cross-slot rheology of polymers," Ph.D. thesis, University of Cambridge, 2006.

Coventry, K. D., and M. R. Mackley, "Cross-slot extensional flow of polymer melts using a multi-pass rheometer," J. Rheol. **52**, 401–415 (2008).

Crosby, B. J., M. Mangnus, W. de Groot, R. Daniels, and T. C. B. McLeish, "Characterization of long chain branching: Dilution rheology of industrial polyethylenes," J. Rheol. **46**, 401–426 (2002).

Crowley, D. G., F. C. Frank, M. R. Mackley, and R. G. Stephenson, "Localised flow birefringence of polyethylene oxide solutions in a four roll mill," J. Polym. Sci., Part B: Polym. Phys. **140**(6), 1111–1119 (1976).

Das, C., N. J. Inkson, D. J. Read, and M.A. Kelmanson, "Computational linear rheology of general branch-on-branch polymers," J. Rheol. **50**, 207–234 (2006).

Dealy, J. M., "Do polymeric liquids exhibit strain hardening?," J. Rheol. **34**(7), 1133–1147 (1990).

den Doelder, C. F., R. Koopmans, M. Dees, and M. Mangnus, "Pressure oscillations and periodic extrudate distortions of long-chain branched polyolefins," J. Rheol. **49**(1), 113–126 (2005).

Frank, F. C., and M. R. Mackley, "Localized flow birefringence of polyethylene oxide solutions in a two roll mill," J. Polym. Sci., Part A-2 **14**, 1121–1131 (1976).

Gabriel, C., and H. Münstedt, "Strain hardening of various polyolefins in uniaxial elongation flow," J. Rheol. **47**(3), 619–630 (2003).

Hassell, D. G., D. Auhl, T. C. B. McLeish, O. G. Harlen, and M. R. Mackley, "The effect of viscoelasticity on stress fields within polyethylene melt flow for a cross-slot and contraction-expansion slit geometry," Rheol. Acta **47**, 821–834 (2008).

Hassell, D. G. , D. Hoyle, D. Auhl, O. Harlen, M. R. Mackley, and T. C. B. McLeish, "Effect of branching in cross-slot flow: the formation of ′w cusps'," Rheol. Acta **48**, 551–561 (2009).

Hassell, D. G., and M. R. Mackley, "Localised flow induced crystallisation of a polyethylene melt," Rheol. Acta **47**(4), 435–446 (2007).

Hassell, D. G., and M. R. Mackley, "An experimental evaluation of the behaviour of mono and polydisperse polystyrenes in cross-slot flow," Rheol. Acta **48**, 543–550 (2009).

Hertel, D., R. Valette, and H. Münstedt, "Three-dimensional entrance flow of a low-density polyethylene (ldpe) and a linear low-density polyethylene (LLDPE) into a slit die," J. Non-Newtonian Fluid Mech. **153**, 82–94 (2008).

Ide, Y., and J. L. White, "Experimental study of elongational flow and failure of polymer melts," J. Appl. Polym. Sci. **22**, 1061–1079 (1978).

Inkson, N. J., T. C. B. McLeish, O. G. Harlen, and D. J. Groves, "Predicting low density polyethylene melt rheology in elongational and shear flows with Pom-pom constitutive equations," J. Rheol. **43**, 873–896 (1999).

Janeschitz-Kriegl, H., *Polymer Melt Rheology and Flow Birefringence* (Springer, Berlin, 1983).

Kotaka, T., A. Kojima, and M. Okamoto, "Elongational flow opto-rheometry for polymer melts. 1. construction of an elongational flow opto-rheometer and some preliminary results," Rheol. Acta **36**, 646–656 (1997).

Koyama, K., and O. Ishizuka, "Birefringence of polyethylene melt in transient elongational flow at constant strain rate," J. Polym. Sci., Part B: Polym. Phys. **27**, 297–306 (1989).

Laun, H. M., and H. Münstedt, "Comparison of the elongational behaviour of a polyethylene melt at constant stress and constant strain rate," Rheol. Acta **15**(10), 517–524 (1976).

Laun, H. M., and H. Münstedt, "Elongational behaviour of a low density polyethylene melt," Rheol. Acta **17**, 415–425 (1978).

Laun, H. M., and H. Schuch, "Transient elongational viscosities and drawability of polymer melts," J. Rheol. **33**, 119–175 (1989).

Lee, K., M. R. Mackley, T. C. B. McLeish, T. M. Nicholson, and O. G. Harlen, "Experimental observation and numerical simulation of transient "stress fangs" within flowing molten polyethylene," J. Rheol. **45**, 1261–1277 (2001).

Li, J.-M., R. W. Burghardt, B. Yang, and B. Khomami, "Flow birefringence and computational studies of a shear thinning polymer solution in axisymmetric stagnation flow," J. Non-Newtonian Fluid Mech. **74**, 151–193 (2009).

Lord, T. D., L. Scelsi, D. G. Hassell, M. R. Mackley, J. Embery, D. Auhl, O. G. Harlen, R. Tenchev, P. K. Jimack, and M. A. Walkley, "The matching of 3D Rolie-Poly viscoelastic numerical simulations with experimental polymer melt flow within a slit and a cross-slot geometry," J. Rheol. **54**, 355–373 (2010).

Luap, C., M. Karlina, T. Schweizer, and D. C. Venerus, "Limit of validity of the stress-optical rule from polystyrene melts: influence of polydispersity," J. Non-Newtonian Fluid Mech. **138**(2–3), 197–203 (2006).

Mackley, M. R., R. T. J. Marshall, and J. B. A. F. Smeulders, "The multipass rheometer," J. Rheol. **39**, 1293–1309 (1995).

Macosko, C. W., *Rheology, Principles, Measurements and Applications* (Wiley-VCH, New York, 1994).

Macosko, C. W., M. A. Ocansey, and H. H. Winter, "Studies with lubricated planar stagnation dies, J. Rheol. **240**(6), 958–958 (1980).

Martyn, M. T., D. J. Groves, and P. D. Coates, "In process measurements of apparent extensional viscosity of low density polyethylene melts using flow visualization," Plast. Rubber Compos. **29**, 14–22 (2009).

McKinley, G. H., and Sridhar, T., "Filament-stretching rheometry of complex fluids," Annu. Rev. Fluid Mech. **34**, 375–415 (2002).

McLeish, T. C. B., "Molecular rheology of h-polymers," Macromolecules, **21**, 1062–1070 (1988).

McLeish, T. C. B., "Tube theory of entangled polymers," Adv. Phys. **51**, 1379–1527 (2002).

McLeish, T. C. B., and R. G. Larson, "Molecular constitutive equations for a class of branched polymers: The Pom-pom polymer," J. Rheol. **42**, 81–110 (1998).

Meissner, J., "Dehnungsverhalten von Polyäthylen-Schmelzen," Rheol. Acta **10**, 230–242 (1971).

Meissner, J., and J. Hostettler, "A new elongational rheometer for polymer melts and other highly viscoelastic liquids," Rheol. Acta **33**, 1–21 (1994).

Meissner, J., T. Raible, and S. E. Stephenson, "Rotary clamp in uniaxial and biaxial extensional rheometry of polymer melts," J. Rheol. **25**, 1–28 (1981).

Meissner, J., S. E. Stephenson, A. Demarmels, and P. Portmann, "Multiaxial Elongational flows of polymer melts—Classification and experimental realization," J. Non-Newtonian Fluid Mech. **11**, 221–237 (1982).

Minoshima, W., and J. L. White, "Instability phenomena in tubular film and melt spinning of rheologically characterised high density, low density and linear low density polyethylenes," J. Non-Newtonian Fluid Mech. **19**, 275–302 (1986).

Müller, A. J., J. A. Odell, and A. Keller, "Elongational flow and rheology of monodisperse polymers in solution," J. Non-Newtonian Fluid Mech. **30**, 99–118 (1988).

Münstedt, H., "New universal extensional rheometer for polymer melts. Measurements on polystyrene," J. Rheol. **23**(4), 421–436 (1979).

Münstedt, H., and D. Auhl, "Rheological measuring techniques and their relevance for the molecular characterization of polymers," J. Non-Newtonian Fluid Mech. **128**, 62–69 (2005).

Münstedt, H., S. Kurzbeck, and L. Egersdörfer, "Influence of molecular structure on rheological properties of polyethylenes," Rheol. Acta **37**, 21–29 (1998).

Münstedt, H., and H. M. Laun, "Elongational properties and molecular structure of polyethylene melts," Rheol. Acta **20**, 211–221 (1981).

Raible, T., A. Demarmels, and J. Meissner, "Stress and Recovery Maxima in LDPE Melt Elongation," Polym. Bull. **1**(6), 397–402 (1979).

Ramirez, J., and A. E. Likhtman, "Reptate: Rheology of entangled polymers, toolkit for analysis of theory and experiment," http://www.reptate.com, 2007.

Rasmussen, H. K., J. K. Nielson, A. Bach, and O. Hassager, "Viscosity overshoot in the start-up of uniaxial elongation of low density polyethylene melts," J. Rheol. **49**:0 369–381 (2005).

J. F. M. Schoonen, F. H. M Swartjes, G. W. M. Peters, F. P. T. Baaijens, and H. E. H Meijer. A 3d numerical/experimental study on a stagnation flow of a polyisobutylene solution. J. Non-Newtonian Fluid Mech. **79**(2–3), 529–561 (1998).

Schuberth, S., and H. Münstedt, "Transient elongational viscosities of aqueous polyacrylamide solutions measured with an optical rheometer," Rheol. Acta **47**, 139–147 (2008).

Scrivener, O., C. Bernera, R. Cressely, R. Hocquart, R. Sellin, and N. S. Vlaches, "Dynamical behaviour of drag-reducing polymer solutions," J. Non-Newtonian Fluid Mech. **5**, 475–495 (1979).

Sentmanat, M. L., "Miniature universal testing platform: from extensional melt rheology to solid-state deformation behavior," Rheol. Acta **43**(6), 657–669 (2004).

Soulages, J., T. Schweizer, D.C. Venerus abd J. Hostettler, F. Mettler, M. Kroger, and H.C. Ottinger, "Lubricated optical rheometer for the study of two-dimensional complex flows of polymer melts," J. Non-Newtonian Fluid Mech. **150**, 43–55 (2008).

Sridhar, T., V. Tirtaatmadja, D. A. Nguyan, and R. K. Gupta, "Measurement of extensional viscosity of polymer solutions," J. Non-Newtonian Fluid Mech. **40**(3), 271–280 (1991).

Taylor, G. T., "The formation of emulsions in definable fields of flow," Proc. R. Soc. London, Ser. A **146**, 501–523 (1934).

Tenchev, R., O. G. Harlen, P. K. Jimack, and M. K. Walkley, in *Finite Element Modelling of Two- and Three-Dimensional Viscoelastic Polymer Flows in Trends in Engineering Computational Technology*, edited by M. Papadrakakis and B. H. V. Topping (Saxe-Coburg, United Kingdom, 2008), pp. 81–101.

Venerus, D. C., and S. H. Zhu, "Stress and birefringence measurements during the uniaxial elongation of polystyrene melts," J. Rheol. **43**(3), 795–813 (1999).

Verbeeten, W. M. H., G. W. M. Peters, and F. P. T. Baaijens, "Differential constitutive equations for polymer melts: the extended Pom-pom model," J. Rheol. **45**, 823–843 (2001).

Winter, H. H., and C. W. Macosko, "Bennett orthogonal stagnation flow, a framework for steady extensional flow experiments," Rheol. Acta **18**, 323–334 (1979).

Wood-Adams, P. M., and J. M. Dealy, "Using rheological data to determine the branching level in metallocene polyethylenes," Macromolecules **33**, 7481–7488 (2000).

Woods-Adams, P., and S. Costeux, "Thermorheological behaviour of polyethylene: Effects of microstructure and long chain branching," Macromolecules **34**(18), 6281–6290 (2001).

Zimm, B. H., and W. H. Stockmayer, "The dimensions of chain molecules containing branches and rings," J. Chem. Phys. **17**(12), 1301–1314 (1949).